EPJ Web of Conferences **6**, 31001 (2010)
DOI:10.1051/epjconf/20100631001

Intragranular strain field in columnar ice during transient creep regime and relation with the local microstucture

F. Grennerat[1], M. Montagnat[1], O. Castelnau[2], P. Vacher[3], and P. Duval[1]

[1] Laboratoire de Glaciologie et Géophysique de l'Environnement, CNRS/Université Joseph Fourier 38402 Saint-Martin-d'Hères, France
[2] Laboratoire Procédés et Ingénierie en Mécanique et Matériaux, CNRS/Arts et Métiers ParisTech, Paris, France
[3] Laboratoire Systèmes et Matériaux pour la Mécatronique, Polytech Savoie, France

Abstract. Transient effects in the creep of polycrystalline ice could play a crucial role for several ice flows (e.g. interaction between Antarctic ice shelves and ocean tides) and also have a major impact concerning deformation mechanisms of ice. During creep deformation of polycrystalline ice, strong stress and strain-rate intragranular heterogeneities are expected. These heterogeneities come from the very large viscoplastic anisotropy of ice crystals (with essentially a single easy plane for the dislocations to glide) which is responsible for the strong mechanical interaction between adjacent grains [1]. In order to go one step further in the quantitative understanding of this process, and to characterize the development of strain heterogeneities at a microscopic (intragranular) scale, we have performed deformation tests on 2-D polycrystalline ice exhibiting columnar grains with controlled grain size. Specimens were submitted to creep test and transient effects, in which both elastic and viscoplastic responses come in play, are investigated. A Digital Image Correlation (DIC) technique, with spatial resolution far smaller than the mean grain size, has been set to get continuous record of the intragranular displacement field during the test [2]. Experimental parameters have been optimized to improve the precision of the DIC results. In parallel, specimen microstructures were analyzed with an automatic ice texture analyzer, before and after deformation, and post-mortem measurements of local misorientations at the intragranular scale were performed. For the first time in ice, this work presents a direct link between grain orientation, strain localization, and lattice distortion at the intragranular scale.

1 Introduction

The elasto-viscoplatic behaviour of polycrystalline ice (ice Ih, nearly compact hexagonal structure, unique phase naturally present on Earth) is strongly affected by the high viscoplastic anisotropy of the ice crystal. The equivalent stress requested for non basal slip is about 60 times the one for basal slip at the same strain rate. Due to this high viscoplastic anisotropy, at a given stress a monocrystal well oriented for basal slip deforms thousand times faster than an isotropic polycrystal. Consequently, in polycrystals, well oriented grains are expected to deform faster than the other ones and this is at the origin of large internal stresses. For ice polycrystals, the transient creep regime (also called primary creep) is characterized by a strong directional hardening until a strain rate minimum reached at about 1 % deformation (secondary creep). This first strain rate decrease can reach three orders of magnitude, due to the development of the long-range internal stress field [3, 4]. This stress state further induces dynamic recrystallization to occur, during tertiary creep starting right after 1% of strain. A permanent regime is then reached at about 10% strain when dynamic recrystallization balances local strain hardening [5].

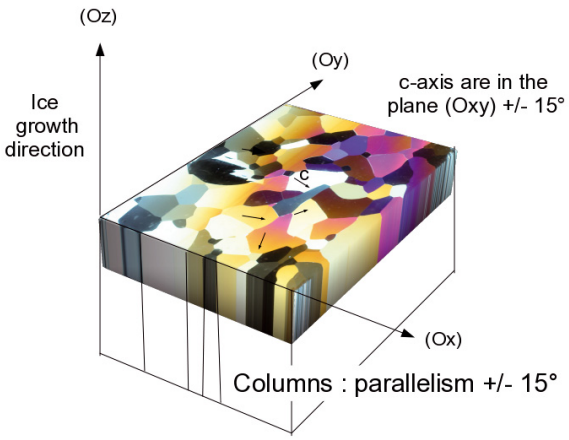

Fig. 1. Typical columnar microstructure obtained under a vertical and uniform temperature gradient. The arrows indicate the c-axis directions

During transient creep, intragranular localization bands appear under polarized light and reveal distorsions of the crystal lattice [6, 7]. If there is two sharp opposite changes in orientation of the active glide surface (the basal planes) over a small area, the lattice distortion observed is defined as a kink band [8, 6]. On the other hand, lattice distortions parallel to the basal plane result from a high local concentration of basal dislocation glide. Such shear bands do not induce any rotation of the *c*-axis. The formation of shear and kink bands have already been observed on two-dimensional columnar Ih ice polycrystals [6, 7]. These localized bands are associated with large internal stresses and their location, intensity and morphology are found to depend on the crystallographic orientation of the grains and on their interaction with neighbouring crystals. Lattice distortions have also been observed and characterized by EBSD with a spatial resolution down to 0.25 µm [7]. Such a fine scale study enabled the determination of the nature of dislocations involved in the kink band formation. A full field formulation based on Fast Fourier Transform was adapted to predict the micromechanical fields for viscoplastic deformation of 2D ice polycrystals [9]. Localized bands as observed by [6] could be qualitatively well predicted.

In the present work we show an original method associating both (i) optical measurements of lattice distortions and (ii) intragranular strain measurements based on a digital image correlation (DIC) technique. The DIC allows estimating the intragranular and intergranular strain field heterogeneity, its evolution with strain, and its correspondance with the specimen microstructure. In Section 2 the DIC technique adapted to compression creep tests is presented. In Section 3 measured strain heterogeneities and lattice distortions are compared to understand the effect of the local internal stress field appearing during the mechanical test. We finally provide a short summary and conclusions in section 4.

2 Digital Image Correlation (DIC) technique adapted to compression creep tests on ice

2.1 Elaboration of columnar ice and microstructure characterization

Samples are made from distilled water with a vertical temperature gradient in order to get a controlled grain size. The cold room is kept at 0 °C and the bottom temperature of the recipient is gradually decreased. With this process, columnar specimen with grain columns nearly parallel to the temperature gradient are obtained (figure 1).

Parallepipedic specimens are machined for compression tests with size of $\approx$ 80 mm $\times$ 80 mm $\times$ 13 mm. A thin section is made before deformation and the microstructure is characterized using an

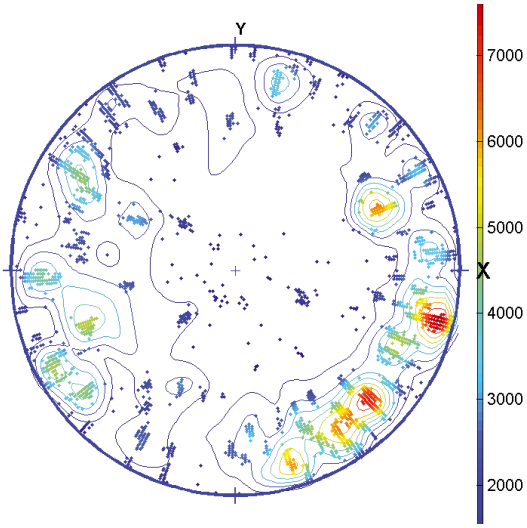

Fig. 2. Schmidt plot of the c-axes before deformation. Y is the loading direction. The color levels indicate a volume fraction (arbitrary units)

automatic ice texture analyzer [10] providing the c-axis orientation (azimuth and colatitude) with a spatial resolution of 43 µm, and an angular resolution of a few degrees. From these orientation data, size and spatial distribution of grains are obtained. c-axis orientations of the sample presented here is provided by a Schmidt plot as presented on figure 2.

2.2 Mechanical test

Uniaxial compression experiments were performed under a constant stress of 0.5 MPa (creep tests), during $\approx$ 30 hours at -10 °C, to reach between 1 and 2% overall strain. Speckle patterns were applied on the surface in order to use a Digital Image Correlation technique to get strain measurements all along the test. The macroscopic vertical displacement was also measured with a LVDT (Low Voltage Displacement Transducer).

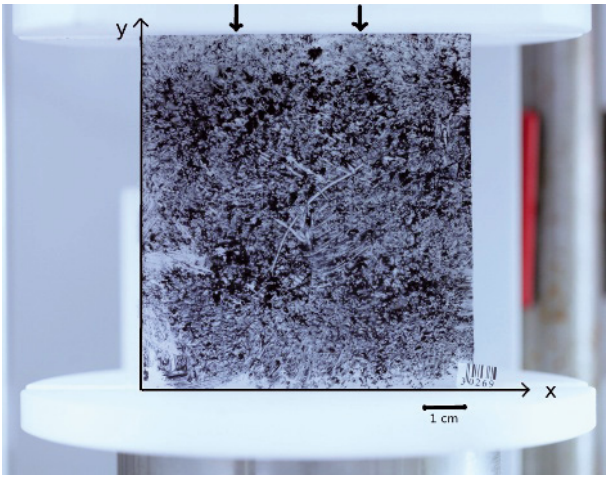

Fig. 3. Sample in test conditions. Arrows represent the loading direction

2.3 Digital Image Correlation

Digital Image Correlation was realized using 7D software [11]. The software provides displacement fields by comparing the speckle patterns between two different images (surfaces). A virtual grid is associated with the initial image, with a grid step of n pixels, and a pattern size of p pixels (here, we choose $p = n$). A bilinear or bicubic interpolation of the gray level function leads to displacement results with a subpixel accuracy, ideally 0.01 pixels for small strains of less than 5% [12]. The displacement field is interpolated with a bi-linear form on each element of the grid. It is differentiated on each element to obtain the strain field (Green-Lagrange tensor). The displacement resolution depends mainly on the DIC algorithm used, the optical material and picture parameters chosen (to reduce the noise), but also on the quality of the speckle applied on the sample surface. The larger the step grid, the better the strain resolution, whereas the spatial resolution deteriorates. In next results, the pixel size was ≈ 0.1 mm. With $n = 16$, the spatial resolution was then 1.6 mm, which is enough compared to the size of our grains (up to 20 mm).

The noise was measured by correlating different pictures without specimen motion. The mean standard deviation measured for displacement norm was ≈ 0.02 pixels with $n = 16$. The displacement resolution is then approximatively 0.02 pixels which corresponds to a strain resolution for a grid step of 16 pixels of 0.3% ($= 0.02/16$). The texture parameters of the speckle were also studied following [13]. The mean standard deviation and auto-correlation radius of the texture were measured (see figure 4). For each sample, the choice of n (grid step and size of the patterns for correlation), the essential parameter in DIC algorithms, can be optimized. Indeed, n has to be small enough to be able to measure very localized deformations, but also large enough so that the standard deviation is sufficient in the correlation window. The autocorrelation radius obtained for $n = 16$ was $R \approx 3.8$ pixels ; it verifies the inequality $2R < n/2$ as it should be.

Out-of-plane effects were not measured specifically but evaluated. The surface roughness after loading is less than 1 mm, a value small enough compared to the distance between the digital camera lens and the sample (90 cm) to lead to negligeable errors on the measured strain in first approximation.

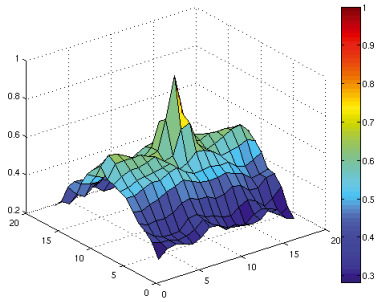

Fig. 4. Autocorrelation surface on a 16x16 pixels zone

3 First results : lattice distortion measurements and evolution of strain heterogeneities

3.1 Microstructure characterization

Since the basal slip plane is almost isotropic in ice crystals (i.e. the direction of basal slip follows the shear stress direction), grain orientation can be characterized by a single Schmid factor, i.e. in the direction for which the resolved shear stress on the basal plane is maximum. Recall however that the Schmid factor definition is associated with an assumption of stress uniformity within the specimen

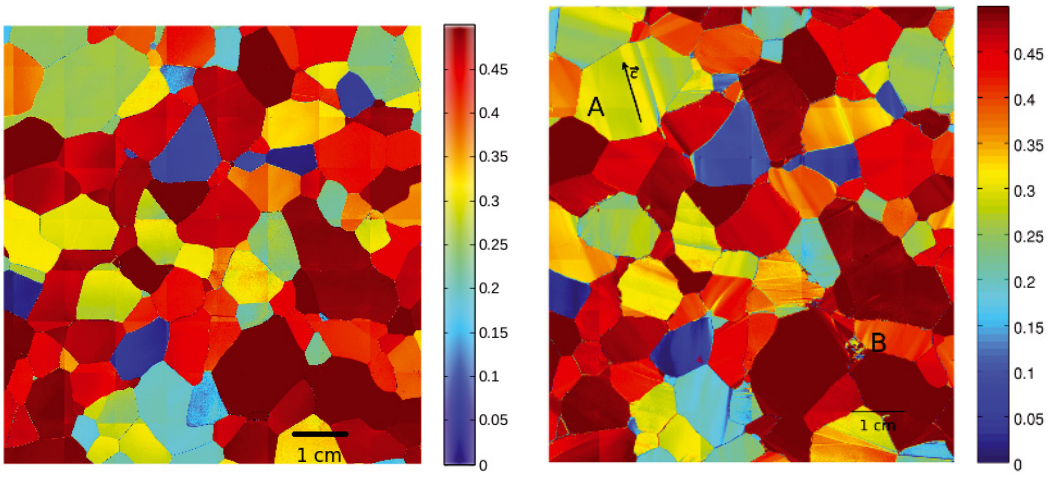

Fig. 5. Schmid factor of the sample (a) before deformation (b) after -1.9% strain. Grains well oriented for basal slip have large Schmid factor (close to 0.5, red).

(Reuss/Sachs bound), not expected here, and therefore this quantity only provides a rough evaluation of which grains are theoretically well or badly oriented for basal slip. In figure 5, well oriented grains have their basal plane (or **c**-axis) close to 45° from the applied macroscopic force. In this figure, note that the observed horizontal and vertical long straight lines are artefacts due to the analyzer and are not to be associated with lattice distortion. Furthermore, for unavoidable pratical reasons, the two analyzed thin sections are a few millimeters apart from each other. Since the columns of the sample are not perfectly parallel, grain shape differences can be observed between both thin sections.

In figure 5, the Schmid factor map is given before deformation and after -1.9% macroscopic strain (mean axial strain). The differences between the two images show the **c**-axis distortions that have developed during the deformation. We cannot access the **a**-axis distortions since the analyzer does not measure them. Consequently basal shear bands are not visible, and the sharp observed bands are subboundaries or kink bands, almost aligned with the **c**-axis orientation (see grain A). Some more continuous distortions inside grains are also observed. Lattice distortions are often initiated at triple junctions and can be observed in most of the grains, as also noticed by [7].

In this sample most of the grains are well oriented for basal slip (see figure 2. Consequently, the specimen deformed faster than usual ones (1% deformation reached in 22 hours instead of 40 hours as usual). In the lower right region of the specimen (marked B in figure 5), dynamic recrystallization occurred during the test, clearly visible through a high density of small new grains currently appearing at triple junctions and grain boundaries. The vast majority of the specimen remained however unaffected by recrystallization processes.

3.2 Evolution of strain heterogeneities

The Von Mises equivalent strain measured by DIC and normalized by the corresponding macroscopic value is shown in figure 6 (a) and (b) at two different deformation stages, namely -0.9% and -1.9% macroscopic axial strain. For a better visualization of the deformations, we plotted the logarithm (base 10) of the equivalent normalized strain. On the colorbar, the 0 level indicates deformations that are equal to the mean equivalent deformation. The largest equivalent deformations are up to 15 times the mean value on the borders, and up to 6 times inside. The high strain zones on the top and bottom sides are probably due to boundary conditions, although thin teflon sheets have been placed between the specimen and the press stages to get rid of contact friction issues. In figure 7(a) is shown the shear strain component ϵ_{xy}, and in figure 7(b) the axial strain component ϵ_{yy} for comparison. In particular, the

shear strain includes deformation created by shear bands, with a high localization of basal dislocation glide.

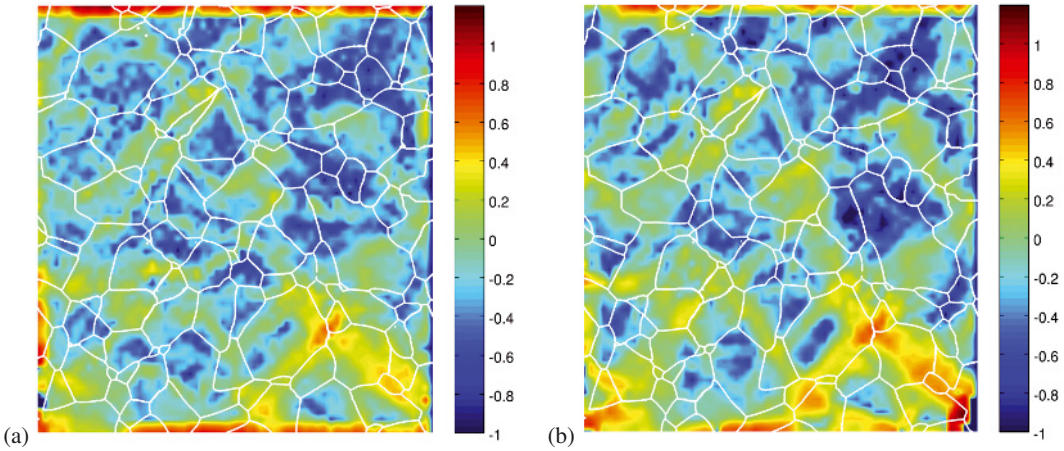

Fig. 6. (a) $log_{10}(\frac{Eeq}{<Eeq>})$ obtained for a macroscopic axial strain of -0.9% ; $< Eeq >\approx 1\%$. (b) $log_{10}(\frac{Eeq}{<Eeq>})$ obtained for a macroscopic axial strain of -1.9% ; $< Eeq >\approx 2.3\%$.

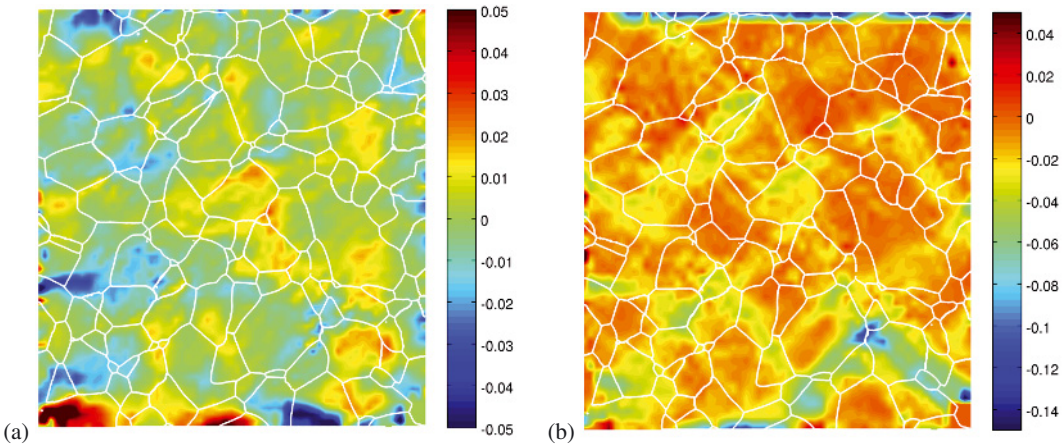

Fig. 7. (a) Shear strain ϵ_{xy} and (b) axial strain ϵ_{yy}, both for a macroscopic axial strain of -1.9%.

At the sample scale, deformation is clearly localized in bands oriented at $+/-45°$ from the applied stress. These bands develop with strain, and get sharper as strain increases, as also observed in several metallic alloys [14]. The band localization is clearly linked with the specimen microstructure: strong localization is essentially observed at grain boundaries, and localization bands take a path through grains well oriented for basal slip. Strain localization seems also often higher at grains boundaries between well oriented and badly oriented grains. Such localization is at the origin of the lattice distortions visible in figure 5 forming sharp subboundaries or kink bands. It can also be observed that B area, where recrystallization was found (see figure 5), is at the intersection of two sharp localization bands. The equivalent deformation reaches there 6 times the mean one. This grain is surrounded by larger grains exhibiting a high Schmid factor. We expect such a configuration to induce very large local internal stresses at the origin of a high level of intragranular strain.

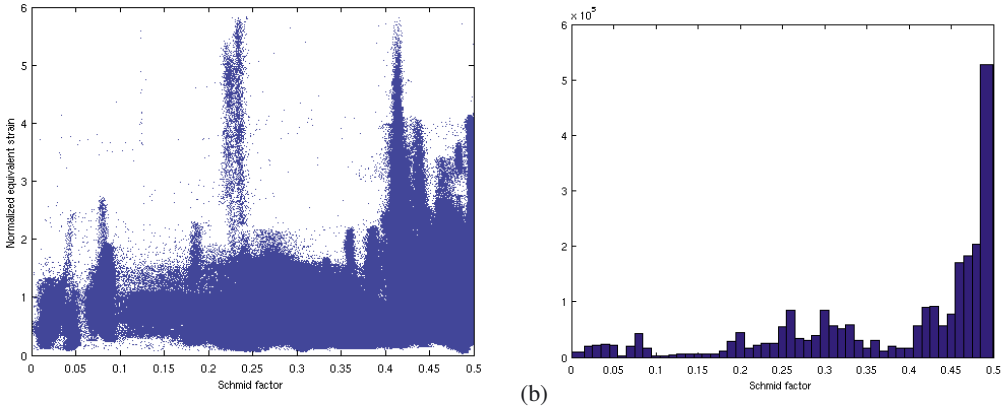

(a) (b)

Fig. 8. (a) Normalized equivalent strain versus Schmid factor (b) Schmid factor histogramm

The correlation between the normalized equivalent strain and the Schmid factor is presented in figure 8 (a). In this plot, each point represents a pixel of the region of interest which has been taken slightly smaller than the entire specimen in order to exclude the side effects on the top and bottom of the specimen. For this analysis, we also removed the "bad" pixels for which the quality of the analyzer results was not sufficient. For comparison, the histogram of Schmid factors is given in figure 8 (b). Although the results are biased by the fact that most of the grains have high Schmid factors in this sample, a large variability is observed in the results. Most of the pixels with the largest strains exhibit high Schmid factor values, but there is also large strain occuring in grains that are not specifically well oriented. For example, an intense deformation peak where strain is as large as 6 times the mean value is obtained for a Schmid factor of about 0.23, i.e. a relatively "hard" grain; this corresponds in fact to pixels belonging to zone B mentioned above in which recrystallization occurred. On the other hand, not all well oriented grains exhibit significant deformation. A significant fraction of grains with Schmid factor of ≈ 0.5 deforms not more than the hardest grains of the specimen. It can be noted that similar results have been obtained numerically with polycrystal micromechanical models adapted to a highly anisotropic viscoplastic mineral [15].

4 Conclusion and perspectives

The DIC method is appropriate to quantify the development of intragranular strain heterogeneity during transient creep as evidenced in this work. The combination of DIC observations and local lattice distortion measurements allows characterizing the nature of the local deformations (shear or kink bands). In particular, the presented results clearly point out the impact of high internal stresses to induce strong lattice distortions as a result of high level of local strain that can reach up to 6 times the average strain. Such a localization is responsible for early occurrence of dynamic recrystallization mechanisms such as new grains nucleation. Deformation bands mainly propagate close to grain boundaries and within grains in which kink and shear bands appear. They tend to follow a macroscopic orientation of about 45° compared with the imposed stress. Although most of the deformation concentrates into favorably oriented areas, large strains can also be reached in grains that are badly oriented for basal slip. Such results reveal the impact of local internal stresses on the intragranular strain field. The present experimental results strongly support the model results obtained for ice polycrystal using a viscoplastic Fast Fourier Transform scheme [9] : the strain field predicted for the considered microstructure (Voronoi tesselation) is in good qualitative agreement with the one presented here.

These results will be implemented to improve recent modeling approaches of elasto-viscoplatic behavior of polycrystals based on full field FFT elasto-viscoplastic calculations [16].

References

1. P. Duval, M. F. Ashby, and I. Anderman. Rate-controlling processes in the creep of polycrystalline ice. *J. of Phys. Chem.*, 87(21):4066–4074, 1983.
2. B. Pan, K. Qian, H. Xie, and A. Asundi. Two-dimensional digital image correlation for in-plane displacement and strain measurement : a review. *Measurement science and technology*, 20, 2009.
3. M. F. Ashby and P. Duval. the creep of polycrystalline ice. *Cold Reg. Sc. Tech.*, 11:285–300, 1985.
4. O. Castelnau, P. Duval, M. Montagnat, and R. Brenner. Elastoviscoplastic micromechanical modeling of the transient creep of ice. *Journal of Geophysical Research Solid Earth*, 113(B11203), 2008.
5. T. H. Jacka and M. Maccagnan. Ice crystallographic and strain rate changes with strain in compression and extension. *Cold Reg. Sci. Technol.*, 8:269–286, 1984.
6. P. Mansuy, J. Meyssonnier, and A. Philip. Localization of deformation in polycrystalline ice: experiments and numerical simulations with a simple grain model. *Computational Materials Science*, 25(1-2):142–150, 2002.
7. S. Piazolo, M. Montagnat, and J. R. Blackford. Sub-structure characterization of experimentally and naturally deformed ice using cryo-ebsd. *Journal of Microscopy*, 230(3):509–519, 2008.
8. C.J.L. Wilson, J.P. Burg, and J.C. Mitchell. The origin of kinks in polycrystalline ice. *Tectonophysics*, 127:27–48, 1986.
9. R. Lebensohn, M. Montagnat, P. Mansuy, P. Duval, J. Meyssonnier, and A. Philip. Modelling viscoplastic behavior and heterogeneous intracrystalline deformation of columnar ice polycrystals. *Acta Materialia*, 52(18):5347–5361, 2009.
10. D. S. Russell-Head and C.J.L. Wilson. Automated fabric analyser system for quartz and ice. *J. Glaciol.*, 24(90):117–130, 2001.
11. P. Vacher, S. Dumoulin, F. Morestin, and S. Mguil-Touchal. Bidimensional strain measurement using digital images. *Proc Instn Mech Engrs*, 213:811–817, 1999.
12. H. Louche, K. Bouabdallah, P. Vacher, T. Coudert, and P. Balland. Kinematic fields and acoustic emission observations associated with the portevin le châtelier effect on an al-mg alloy. *Experimental Mechanics*, 48:741–751, 2008.
13. Karen Triconnet, Katell Derrien, FranÃ§ois Hild, and Didier Baptiste. Parameter choice for optimized digital image correlation. *Optics and Lasers in Engineering*, 47:728–737, 2009.
14. E. Héripré, M. Dexet, J. Crépin, L. Gélébart, A. Roos, M. Bornert, and D. Caldemaison. Coupling between experimental measurements and polycrystal finite element calculations for micromechanical study of metallic materials. *International Journal of Plasticity*, 23(9):1512 – 1539, 2007.
15. O. Castelnau, R.A. Lebensohn, P. Ponte Casta neda, and D.K. Blackman. Earth Mantle Rheology inferred from Homogenization Theories*, Multi-scale modeling of heterogeneous materials*. 2008.
16. H. Moulinec and P. Suquet. Intraphase strain heterogeneity in nonlinear composites: acomputational approach. *European Journal of Mechanics - A/Solids*, 22(5):751 – 770, 2003. General and plenary lectures from the 5th EUROMECH Solid Mechanics Conference.